Behavioral/Systems/Cognitive

Striatal Dopamine D_2/D_3 Receptors Mediate Response Inhibition and Related Activity in Frontostriatal Neural Circuitry in Humans

Dara G. Ghahremani,[1] Buyean Lee,[1] Chelsea L. Robertson,[2] Golnaz Tabibnia,[3] Andrew T. Morgan,[1] Natalie De Shetler,[1] Amira K. Brown,[1] John R. Monterosso,[4] Adam R. Aron,[5] Mark A. Mandelkern,[6] Russell A. Poldrack,[7] and Edythe D. London[1,2,8]

Departments of [1]Psychiatry and Biobehavioral Sciences and [2]Molecular and Medical Pharmacology, and [8]Brain Research Institute, University of California, Los Angeles, Los Angeles, California 90095, [3]Department of Social and Decision Sciences, Carnegie Mellon University, Pittsburgh, Pennsylvania 15212, [4]Department of Psychology, University of Southern California, Los Angeles, California 90089, [5]Department of Psychology, University of California, San Diego, La Jolla, California 92093, [6]Department of Physics, University of California, Irvine, Irvine, California 92697, and [7]Departments of Psychology and Neurobiology, University of Texas, Austin, Texas 78712

Impulsive behavior is thought to reflect a traitlike characteristic that can have broad consequences for an individual's success and well-being, but its neurobiological basis remains elusive. Although striatal dopamine D_2-like receptors have been linked with impulsive behavior and behavioral inhibition in rodents, a role for D_2-like receptor function in frontostriatal circuits mediating inhibitory control in humans has not been shown. We investigated this role in a study of healthy research participants who underwent positron emission tomography with the D_2/D_3 dopamine receptor ligand [^{18}F]fallypride and BOLD fMRI while they performed the Stop-signal Task, a test of response inhibition. Striatal dopamine D_2/D_3 receptor availability was negatively correlated with speed of response inhibition (stop-signal reaction time) and positively correlated with inhibition-related fMRI activation in frontostriatal neural circuitry. Correlations involving D_2/D_3 receptor availability were strongest in the dorsal regions (caudate and putamen) of the striatum, consistent with findings of animal studies relating dopamine receptors and response inhibition. The results suggest that striatal D_2-like receptor function in humans plays a major role in the neural circuitry that mediates behavioral control, an ability that is essential for adaptive responding and is compromised in a variety of common neuropsychiatric disorders.

Introduction

Poor ability to inhibit an ongoing response (response inhibition) is manifested in several psychiatric disorders involving impulsive behavior (Moeller et al., 2001; Aron et al., 2007b; Chamberlain and Sahakian, 2007; de Wit, 2009). Such disorders have been associated with dopaminergic dysfunction (Swanson et al., 2007; Koob and Volkow, 2010), suggesting that dopamine contributes to response inhibition. This view is supported by pharmacological findings (de Wit et al., 2002; Eagle and Robbins, 2003b; Eagle et al., 2011), evidence that links dopamine-related genetic polymorphisms with response inhibition (Congdon et al., 2008; Hamidovic et al., 2009), and demonstrations of impaired response inhibition in stimulant abusers (Monterosso et al., 2005; Colzato et al., 2007), who have low striatal dopamine D_2-like receptor availability (Volkow et al., 2001; Lee et al., 2009).

Rodent studies using the Stop-signal Task (SST) (Verbruggen and Logan, 2008) to assess response inhibition have suggested a specific role of dopamine D_2/D_3 receptors in the dorsal striatum (Eagle et al., 2011). Although a relationship between response inhibition and dopaminergic neurochemical markers has not been established in humans, dopamine receptors have been linked to self-report measures of impulsivity. Impulsivity has been correlated negatively with striatal dopamine D_2/D_3 receptor availability in a combined sample of methamphetamine-dependent and healthy control participants (Lee et al., 2009) and positively with amphetamine-induced striatal dopamine release in healthy participants (Buckholtz et al., 2010). These findings highlight the relevance of striatal dopamine in trait-like impulsivity without elucidating its relationship to behavioral measures of response inhibition.

Studies of SST performance in patients and functional magnetic resonance imaging (fMRI) responses in healthy controls have highlighted the importance of fronto-basal ganglia circuitry

Received August 17, 2011; revised March 23, 2012; accepted March 29, 2012.

Author contributions: D.G.G., B.L., G.T., J.R.M., A.R.A., R.A.P., and E.D.L. designed research; D.G.G., B.L., C.L.R., G.T., A.T.M., N.D.S., A.K.B., J.R.M., M.A.M., and E.D.L. performed research; D.G.G., B.L., C.L.R., and A.T.M. analyzed data; D.G.G., A.R.A., R.A.P., and E.D.L. wrote the paper.

This work was supported by National Institutes of Health (NIH) Grants P20 DA022539 and R01 DA020726 (E.D.L.), the Consortium for Neuropsychiatric Phenomics NIH Roadmap for Medical Research Grants UL1 DE019580 and RL1 DA024853 (E.D.L.), and University of California at Los Angeles General Clinical Research Center Grant M01 RR00865. Additional funding was provided by endowments from the Thomas P. and Katherine K. Pike Chair in Addiction Studies and the Marjorie M. Greene Trust.

The authors declare no competing financial interests.

Correspondence should be addressed to either Dr. Dara Ghahremani or Dr. Edythe London, UCLA Semel Institute, 740 Westwood Plaza, C8-831, Los Angeles, CA 90095. E-mail: darag@ucla.edu or elondon@mednet.ucla.edu.

DOI:10.1523/JNEUROSCI.4284-11.2012

 0270-6474/12/327316-09$15.00/0

in response inhibition (Rieger et al., 2003; Aron et al., 2007b; Chambers et al., 2009), emphasizing the role of right inferior frontal cortex (IFC), anterior insula, presupplementary motor area (pre-SMA)/anterior cingulate, and the subthalamic nucleus (STN) (Swann et al., 2011; Mirabella et al., 2012). It has been proposed that the right IFC and/or pre-SMA project to the STN through a "hyperdirect" pathway to stop a response quickly (Aron et al., 2007a). However, striatal activation also accompanies stopping (Vink et al., 2005; Aron and Poldrack, 2006; Li et al., 2008; Boehler et al., 2010; Zandbelt and Vink, 2010), possibly reflecting inhibitory control in preparation for stopping or occurring through an "indirect" basal ganglia pathway. Further insights may come from exploring the relationship between frontostriatal activation during stopping and dopaminergic markers.

To determine how D_2/D_3 receptors relate to response inhibition and associated frontostriatal activation, we assessed striatal D_2/D_3 receptor availability using positron emission tomography (PET) in healthy participants who performed the SST during fMRI. As suggested by the aforementioned studies, we anticipated a negative correlation of striatal D_2/D_3 receptor availability with stopping speed. We also expected that striatal D_2/D_3 receptor availability would be related to the fMRI response during stopping. Although the literature directly linking dopaminergic neurochemical markers with human fMRI responses is sparse, striatal dopamine release has been positively correlated with striatal fMRI activation, suggesting a positive relationship between D_2/D_3 receptor availability and response inhibition-related striatal fMRI activation (Schott et al., 2008).

Materials and Methods

Research participants

All procedures were approved by the UCLA Office for the Protection of Research Subjects. Participants were recruited using radio, internet, and local newspaper advertisements. After receiving a detailed explanation of the study, participants gave written informed consent and underwent eligibility screening using questionnaires, the Structured Clinical Interview for *Diagnostic and Statistical Manual of Mental Disorders*, fourth edition (DSM-IV) Axis I Disorders (First et al., 2002), and medical examination. Participants were excluded from the study for the following criteria: current Axis I diagnosis other than nicotine dependence; use of psychotropic medications or substances, except some marijuana or alcohol (not meeting DSM-IV criteria for dependence); CNS, cardiovascular, pulmonary, or systemic disease; HIV seropositivity, hepatic disease, or hematocrit <32; pregnancy; lack of fluency in English; and MRI ineligibility due to metal implants or claustrophobia. Corrective lenses were used to ensure adequate visual acuity when participants viewed stimuli in the scanner. Participants were required to provide negative urine samples for illicit drugs of abuse on days of testing. They received compensation in the form of cash, gift certificates, and vouchers.

Twenty-one healthy adults participated in the study. Data from three participants were excluded from analyses because the participants did not meet performance criteria on the Stop-signal Task. To be included, participants were required to meet the following criteria: successful inhibition on 40–60% of stop trials, at least 80% responding on Go trials, <10% errors in discriminating the arrow direction on Go trials, and an estimated Stop-signal reaction time (SSRT) >50 ms. All three excluded participants responded on <80% of Go trials and had SSRT estimates of <50 ms (unrealistically fast, suggesting erroneous task performance); one had >10% errors on direction discrimination. In total, data from 18 participants were included in the reported analyses [age, 32.5 ± 8.2 years (mean ± SD); 8 women, 10 men].

Stop-signal task and fMRI design

During scanning, participants performed the Stop-signal Task (Logan and Cowan, 1984), which required them to execute a motor response (Go trials) on most trials and to withhold their response on some trials (Stop trials). The task implemented was similar to the one used by Aron and Poldrack (2006) except that two adaptive staircases were used instead of four (see below). On each trial, a left- or right-pointing arrow stimulus was displayed. On Go trials (75% of trials), participants were to respond as quickly as possible with a left or right key press (using index and middle fingers of the right hand). For the Stop trials (25% of trials), participants were instructed to stop their response when they heard a Stop signal (an auditory tone) that was presented at a particular delay [stop-signal delay (SSD)] subsequent to the arrow stimulus. The SSD value for the Stop trial was adaptively determined to ensure that participants inhibited their response successfully on ~50% of trials.

Performance on the Stop-signal Task has been characterized as a race between independently running Go and Stop processes (Logan and Cowan, 1984). Although Go response times are directly measurable (Go RT), Stop response times are not and must be estimated using the SSRT. The SSRT is computed by subtracting the SSD from the Go RT and relies on the assumption that the response-time distribution on Stop trials is the same as on Go trials. Using the staircase procedure to adjust the SSD dynamically for producing inhibition on 50% of Stop trials ensures consistency with this assumption and accounts for differences in Go RTs across participants (Band et al., 2003).

A Go trial consisted of the following sequence. First, a white circular fixation ring (subtending a 4.3 × 6.2° viewing angle) appeared in the center of the screen against a black background. After 500 ms, a white arrow appeared within the fixation circle. The arrow pointed to the left on half the trials and to the right on the other half. The direction of the arrow was randomized across trials. The fixation ring and arrow remained on the screen for up to 1 s, after which they disappeared and the background was shown. The fixation ring and arrow disappeared as soon as the participant made a choice, and the background was shown for the remainder of the 1 s period plus the rest period. If the participant pressed the incorrect key in response to the arrow, the computer recorded the error, but no feedback was provided to the participant. A Stop trial was identical to a Go trial in all respects, except that a tone (900 Hz; duration, 500 ms) was played at the SSD after onset of the arrow stimulus. If a participant inhibited his or her response on Stop trials, the arrow and fixation ring remained on the screen for the duration of the 1 s period. If the participant responded, the arrow and fixation ring disappeared, and the background screen was shown for the remaining period. The SSD fluctuated dynamically throughout the experiment, depending on the participant's performance. If a participant successfully inhibited a response on a Stop trial, inhibition was made more difficult on a subsequent Stop trial by increasing the SSD by 50 ms; if a participant did not successfully inhibit, inhibition was made easier by decreasing the SSD by 50 ms. Two independent staircases were used in this way. Starting SSD values were determined on the basis of each participant's performance of the task outside the scanner in a behavioral testing session on a previous day [SSD, 256.1 ± 106.5 (mean ± SD)].

On the scanning day, both staircases began at the same SSD value, determined for each participant in the earlier behavioral test session. Two blocks (fMRI runs) of trials were presented, with 96 Go trials and 32 Stop trials in each block. Each SSD staircase was incremented or decremented 16 times within each block. The staircases were independent but randomly interleaved (i.e., each particular Stop trial was randomly selected from one of the two staircases). To maintain continuity of performance between the two blocks, the starting SSD values for the two ladders in the second block were set to the last SSD values from the ladders in the previous block.

We used custom MATLAB (MathWorks) code to select sequences of Go and Stop events and to select the distribution of rest time in a way that optimized the detection of hemodynamic responses for the critical contrast of Stop and Go events. Approximately four Go trials appeared between Stop trials [4.08 ± 2.97 (mean ± SD)], and the number of leftward and rightward pointing arrows was equal. Rest periods were imposed after each trial. The duration of rest time ranged between 0.5 and 4 s (mean, 1 s; sampled from an exponential distribution truncated at 4 s). A Monte Carlo approach was used to generate a large number of sequences

within these constraints to select those with the highest efficiency for detecting differences between Go and Stop events (Liu et al., 2001).

The presentation of all stimuli and response collection were programmed using MATLAB (MathWorks) and the Psychtoolbox on a MacBook running Mac OSX (Apple). Visual and auditory stimuli were presented using MRI-compatible goggles and headphones, respectively (Resonance Technologies).

Procedure

Task directions were explained to participants on their prescan behavioral testing day. They were informed that stopping and going were equally important and that it would not always be possible to stop. Within the scanner, participants responded with their right hands on an MRI-compatible button box. Stop tones were played through headphones at a level both sufficient to exceed scanner noise and comfortable to the subject. Each scan was preceded by an instruction screen with a reminder to the subject: "Remember, respond as FAST as you can once you see the arrow. However, if you hear a beep, your task is to STOP yourself from pressing. Stopping and going are equally important."

MRI. Imaging was performed using a 3 T Siemens AG Allegra MRI scanner. We acquired 364 functional T2*-weighted echoplanar images (EPI) across two runs [slice thickness, 4 mm; 34 slices; repetition time (TR), 2 s; echo time (TE), 30 ms; flip angle, 90°; matrix, 64 × 64; field of view (FOV), 200 mm]. Two additional volumes at the beginning of each run were discarded to allow for T1 equilibrium effects. For registration purposes, a T2-weighted, matched-bandwidth, high-resolution anatomical scan (same slice prescription as EPI) and a magnetization-prepared, rapid-acquisition, gradient-echo (MPRAGE), high-resolution scan were acquired for each participant. The MPRAGE scan was conducted in a separate session on a Siemens Sonata 1.5T scanner (slice thickness, 1 mm; 160 slices; TR, 1900 ms; TE, 4.38 ms; flip angle, 15; FOV, 256 mm). The orientation for matched bandwidth and EPI scans was oblique axial so as to maximize full brain coverage and to optimize the signal from brain regions prone to signal dropout.

PET. Dopamine D_2/D_3 receptor availability was assayed using [^{18}F]fallypride, a radioligand with high affinity for D_2/D_3 receptors (Mukherjee et al., 1995). Images were acquired using a Siemens ECAT EXACT HR+ scanner [in-plane resolution full-width at half-maximum (FWHM), 4.6 mm; axial FWHM, 3.5 mm; axial FOV, 15.52 cm] in three-dimensional (3D) mode. Subjects were placed in the supine position with the brain centered in the transaxial field of view. A 7 min transmission scan was acquired using a rotating ^{68}Ge/^{68}Ga rod source for attenuation correction. PET dynamic data acquisition was initiated with a bolus injection of [^{18}F]fallypride (~5 mCi in 30 s). To reduce radiation exposure to the bladder wall and to minimize discomfort, participants were allowed a 20 min break after the first 80 min of emission data acquisition and then returned to the scanner bed after the break. After a second 7 min transmission scan, emission data were collected for another 80 min. The total dynamic scanning sequence consisted of six 30 s frames, seven 1 min frames, five 2 min frames, four 5 min frames, and twelve 10 min frames. Data were reconstructed using ECAT v7.3 OSEM (Ordered Subset Expectation Maximization; 3 iterations, 16 subsets) after corrections for decay, attenuation, and scatter.

Data analysis

Behavioral analyses. The median and SD of Go response times (Go RT) were calculated for each participant, as were the percentage of Go responses and the percentage of inhibition on Stop trials. The average SSD was computed for each subject from the values of the two staircases, and, because the 50% inhibition criteria were met, SSRT was estimable by subtracting each participant's average SSD from his or her median Go RT. All behavioral data were analyzed using MATLAB (MathWorks) and the R statistical package (R Development Core Team, 2011).

fMRI image analyses. Analysis of fMRI data was performed using the FSL (v4.1) toolbox from the Oxford Centre for fMRI of the Brain. The image time course for each participant was first realigned to compensate for small head movements (Jenkinson et al., 2002), and all nonbrain matter was removed using the FSL brain extraction tool. Images were denoised for motion-related artifacts using independent components analysis (FSL MELODIC). Motion-related components were identified manually using a set of heuristics (Tohka et al., 2008), and the data were then reconstructed after removing the motion-related components. Data were spatially smoothed using a 6 mm FWHM Gaussian kernel. Registration was conducted through a three-step procedure, whereby EPI images were first registered to the matched-bandwidth, high-resolution structural image, then to the MPRAGE structural image, and finally into standard [Montreal Neurological Institute (MNI)] space (MNI avg152 template) using 12-parameter affine transformations (Jenkinson and Smith, 2001). Registration from MPRAGE structural images to standard space was further refined using FNIRT nonlinear registration (Andersson et al., 2007a,b). Statistical analyses at the single-subject level were performed in native space, with the statistical maps normalized to standard space before higher-level analysis.

Whole-brain statistical analysis was performed using a multistage approach to implement a mixed-effects model treating participants as random-effects variables. Statistical modeling was first performed separately for each imaging run. Regressors of interest were created by convolving a delta function, representing trial onset times with a canonical (double gamma) hemodynamic response function. Regressors of interest included Go trials, Successful Stop trials, and Unsuccessful Stop trials. Go trials in which participants omitted a response or made discrimination errors were modeled using a single nuisance covariate, and motion parameters were included as covariates of no interest to account for variance associated with residual motion not captured by the MELODIC denoising procedure. No participant exceeded translational motion above 2.5 mm [0.49 ± 0.39 (mean ± SD)].

For all analyses, time-series statistical analysis was performed using FILM (FMRIB Improved Linear Model) with local autocorrelation correction (Woolrich et al., 2001) after high-pass temporal filtering (Gaussian-weighted LSF straight-line fitting, with $\sigma = 33$ s). Contrast images for the two runs within each session were combined using fixed-effects analyses. The results of these contrasts were submitted to whole-brain correlations with D_2/D_3 receptor binding-potentials (see Statistical analyses).

Structural MRI processing and volume of interest analyses. The caudate nucleus, putamen, and nucleus accumbens were defined as volumes of interest (VOIs) using an automated procedure (FSL FIRST; FMRIB Integrated Registration and Segmentation Tool; Oxford University, Oxford, UK; www.fmrib.ox.ac.uk/fsl/first/index.html) that provides a 3D binary mask for these regions in native space. The caudate nucleus VOI included the head and body of caudate, and the putamen VOI included the entire putamen.

PET image analyses. Reconstructed PET images were combined into 16 images, each containing an average of 10 min dynamic frames of data. These 16 images were motion corrected using the FSL McFLIRT (Jenkinson et al., 2002) (using least squares as the cost function and the first image of the second scanning block as the reference volume). After motion correction, PET images were coregistered to the participant's structural MRI using a six-parameter, rigid-body transformation computed with the ART software package (Ardekani et al., 1995). Specifically, the transformation matrix for registration of the first PET image (containing maximal intensities across the brain) to the MRI was computed and applied to all 16 PET images in the series. Time–activity data within anatomically defined VOIs (see above) were extracted from motion-corrected, coregistered PET data and imported into the PMOD v3.2 (PMOD Technologies) kinetic analysis program for kinetic modeling. Time–activity curves were fit using the simplified reference tissue model (SRTM) (Lammertsma and Hume, 1996) to provide an estimation of k2′, the rate constant for transfer of the tracer from the reference region to plasma. The cerebellum was used as a reference region, a common practice that assumes the cerebellum is devoid of specific binding sites for the radiotracer (Lammertsma and Hume, 1996). Although non-negligible D_2-like receptor binding in cerebellum has been measured using [^{11}C]FLB457, specific binding of [^{18}F]fallypride (which has a higher equilibrium dissociation constant) was not detected in the cerebellum (Vandehey et al., 2010). A volume-weighted average of k2′ estimates from high-activity regions (caudate and putamen) was computed. The time–activity curves were refit using the SRTM2 model (Wu and

Carson, 2002) with the computed k2′ values applied to all VOIs. Binding potential (BP_{ND}) was then calculated by subtracting 1.0 from the product of the tracer delivery (R1) and the tracer washout (k2′/k2a). Whole-brain BP_{ND} maps were computed by performing the above computations on a voxel-by-voxel basis.

Given that BP_{ND} values in the left and right regions of each striatal VOI were highly correlated (caudate: $r = 0.99$, $p < 0.001$; putamen: $r = 0.89$, $p < 0.001$; nucleus accumbens: $r = 0.71$, $p < 0.001$), a volume-weighted average of the left and right portion of each VOI was used for correlation analyses. Volume-weighted averages of left and right striatal VOI Successful Stop versus Go fMRI parameter estimates were also computed because they were also highly correlated (caudate: $r = 0.82$, $p < 0.0001$; putamen: $r = 0.81$, $p < 0.0001$; nucleus accumbens: $r = 0.66$, $p < 0.005$).

Statistical analyses

We used both VOI-based and voxelwise approaches to examine correlations between BP_{ND} in striatal regions, SSRT, and the fMRI contrast of Successful Stop versus Go. VOI-based correlations were computed using the nonparametric Spearman's ρ test for consistency with the nonparametric whole-brain correlations (VOI results were comparable to those obtained using Pearson correlations). To obtain sensitivity in substructures within VOIs, BP_{ND} images (thresholded to exclude voxels with negligible D_2/D_3 binding, i.e., $BP_{ND} < 1$) were subjected to linear regression to test associations with SSRT. Control for familywise error was implemented using nonparametric randomization tests with the FSL RANDOMISE v2.8 tool (permutation-based nonparametric inference; Oxford University), with variance smoothing of 10 mm (FWHM Gaussian) (www.fmrib.ox.ac.uk/fsl/randomise). This method repeatedly reorders the rows of the design matrix and computes the statistical map for each sample, recording the maximum statistic across the brain for each sample to obtain an empirical null distribution (Nichols and Holmes, 2002). Threshold-free cluster enhancement (TFCE) (Smith and Nichols, 2009) was used to detect significant clusters of activation. For each analysis, 5000 randomization runs were performed. Statistical maps were thresholded at $p < 0.05$ (one-tailed) corrected for the entire search volume, though some results are shown at more lenient thresholds for visualization purposes, as noted in the Results section.

In addition to VOI-based correlations between striatal binding potentials and successful Stop versus Go fMRI parameter estimates, we conducted whole-brain analyses examining regions throughout the brain that showed a correlation with BP_{ND}. Whole-brain between-subject correlations were conducted using the FMRIB Local Analysis of Mixed Effects module in FSL (Beckmann et al., 2003; Woolrich et al., 2004) using binding-potential values for each VOI as covariates (zero-meaned). Z (Gaussianized T) statistic images were thresholded using cluster-corrected statistics with a height threshold of $Z > 1.96$ and a cluster probability threshold of $p < 0.05$, whole-brain corrected using the theory of Gaussian random fields (Worsley et al., 1992). All analyses were subjected to robust outlier deweighting (Woolrich, 2008). Conjunction analyses to indicate overlap between statistical maps were conducted using the revised minimum statistic approach proposed by Nichols et al. (2005) and cluster-corrected statistics. Locations of cortical activations were identified using the Harvard–Oxford Probabilistic Atlas, which is included in the FSL software package, and the sectional brain atlas of Duvernoy (1999).

Results

Behavior

Behavioral results from the Stop-signal Task are shown in Table 1. Participants performed at 99% correct on Go trials and inhibited their responses on approximately half the Stop trials (51%), indicating that the adaptive staircase procedure for equating Stop trials across participants was successful. SSRT and median Go RT values were similar to those reported in the literature from similar samples (Logan et al., 1997; Boehler et al., 2010).

Table 1. Mean and SD of Stop-signal Task performance variables

	Mean	SD
SSRT (ms)	218	37
Median Go RT (ms)	459	76
SD Go RT (ms)	90	28
Correct Go responding, %	99	0.12
Inhibition on Stop trials, %	51	0.54

$n = 18$.

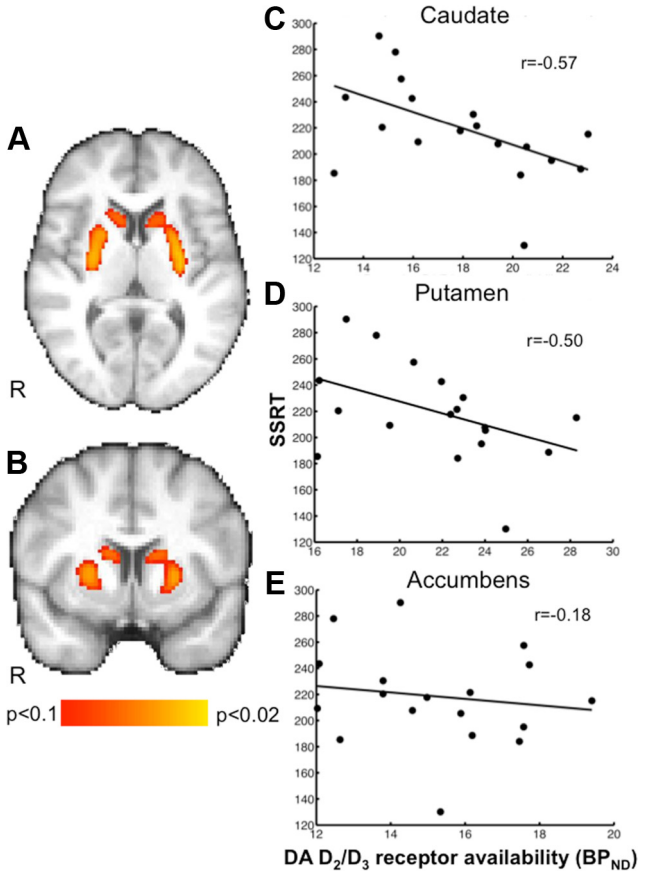

Figure 1. Correlations between striatal dopamine D_2/D_3 receptor availability (BP_{ND}) and SSRT ($n = 18$). Participants who stopped more quickly showed greater D_2/D_3 receptor availability in caudate and putamen. ***A***, ***B***, Results from voxelwise nonparametric regression of BP_{ND} on SSRT. TFCE probability maps (corrected for multiple comparisons) are overlaid on the MPRAGE anatomical image. Maps show SSRT was negatively correlated with BP_{ND} in caudate and putamen but not nucleus accumbens. Voxelwise height threshold is set at $p < 0.1$ for illustration purposes. Images are presented in radiological orientation (right = left). ***C–E***, Scatterplots indicating relationship between SSRT and BP_{ND} extracted from anatomically defined caudate ($p = 0.02$), putamen ($p = 0.04$), and nucleus accumbens ($p = 0.47$) VOIs. Because left and right BP_{ND} values were highly correlated (all $r > 0.71$ and all $p < 0.001$), volume-weighted averages of left and right values were used.

Relation between striatal D_2/D_3 receptor availability (BP_{ND}) and SSRT

SSRT showed a significant negative correlation with BP_{ND} values in the anatomically defined caudate ($r = -0.57$) and putamen ($r = -0.50$) VOIs but not in the nucleus accumbens ($r = -0.18$) (Fig. 1; Table 2), indicating that better response inhibition performance was associated with greater receptor availability. Voxelwise analyses revealed a significant negative correlation bilaterally in the putamen ($p < 0.05$, TFCE corrected for multiple comparisons) and one that approached significance in the caudate ($p < 0.06$, TFCE corrected) (Fig. 1), but correlations in the vicinity of the nucleus accumbens only appeared at lower thresh-

Table 2. Dopamine D_2/D_3 receptor availability (BP_{ND}) values in striatal regions of interest and their correlations with SSRT and Successful Stop versus Go fMRI parameter estimates

	BP_{ND}		BP_{ND} correlation with SSRT		BP_{ND} correlation with SuccStop versus Go fMRI parameter estimates	
Striatal region	Mean	SD	*r*	*p*	*r*	*p*
Caudate	17.85	3.18	−0.57	0.02*	0.82	0.00002***
Putamen	21.72	3.55	−0.50	0.04*	0.27	0.29
Accumbens	15.22	2.19	−0.18	0.47	0.30	0.23

n = 18. *$p < 0.05$; ***$p < 0.0001$. SuccStop, Successful Stop.

olds ($p < 0.15$, TFCE corrected). No correlations were observed between striatal BP_{ND} and median Go RT (caudate: $r = 0.04$, $p = 0.88$; putamen: $r = 0.08$, $p = 0.74$; nucleus accumbens: $r = 0.10$, $p = 0.70$), suggesting that the observed caudate and putamen correlations were specific to variation in inhibiting a response, not to motor engagement in general.

Successful Stop versus Go fMRI and relationship with SSRT

Whole-brain analyses of the Successful Stop versus Go fMRI contrast revealed regions of activation typically reported for this task, including the right inferior frontal gyrus, supplemental motor area/presupplementary motor area, anterior cingulate, bilateral anterior insula, bilateral middle frontal gyrus, bilateral superior temporal gyrus, and bilateral posterior parietal cortex (Fig. 2; Table 3). Among striatal regions, bilateral caudate activation did not survive cluster-corrected thresholds but showed significant activation at an uncorrected threshold of $p < 0.001$. Whole-brain correlation analysis using participants' SSRT values as covariates revealed a negative correlation in clusters of activation within the superior frontal gyrus, anterior cingulate, left inferior frontal gyrus/lateral orbitofrontal cortex, and, on the right side, caudate, putamen, thalamus, and amygdala.

Relation between D_2/D_3 receptor availability (BP_{ND}) and successful Stop versus Go fMRI

VOI-based analyses revealed a significant positive correlation between BP_{ND} and Successful Stop versus Go fMRI activation in the caudate but not in the putamen or nucleus accumbens (Fig. 3*A*,*B*; Table 2). When removing an outlier in the caudate fMRI data (one time point >2 SDs; Fig. 3*B*, scatterplot), the correlation remained significant ($r = 0.79$, $p = 0.0002$, $n = 17$).

To determine the extent to which frontostriatal functional activation related to caudate BP_{ND}, we performed a whole-brain voxelwise correlation of Successful Stop versus Go fMRI activation and caudate BP_{ND} (corrected for multiple comparisons). In addition to the caudate, several regions within the frontal lobes showed significant clusters (Fig. 3*C*,*D*; Table 4); these included the right lateral orbital/frontopolar cortex, left anterior insula, and rostral anterior cingulate/superior frontal gyrus (medial portion), regions previously reported to be related to response-inhibition behavior. A conjunction analysis used to statistically identify the extent to which these regions overlapped with those activated during the Successful Stop versus Go contrast revealed overlap in the rostral anterior cingulate and left anterior insula but at a liberal voxelwise height threshold of $Z > 1$ (cluster probability threshold of $p < 0.05$). A conjunction with the correlation of Successful Stop versus Go and SSRT also showed overlap in rostral anterior cingulate as well as right superior frontal gyrus (medial portion) and left inferior frontal gyrus at the same liberal threshold (for annotations, see Table 3). No regions showed a negative correlation with BP_{ND}.

Discussion

Striatal dopamine receptor availability was associated with both response-inhibition performance and stopping-related frontostriatal activation. Specifically, D_2/D_3 receptor availability in the dorsal, but not the ventral, striatum was negatively correlated with SSRT (i.e., those with greater receptor availability stopped more quickly). These correlations held for SSRT but not for Go RT, suggesting that they were specific to stopping. Caudate D_2/D_3 receptor availability was positively correlated with fMRI Stop versus Go activation in the caudate and prefrontal regions, including right lateral orbitofrontal/frontopolar cortex, left anterior insula, and anterior cingulate cortex.

Dopamine and response inhibition

This study is the first to relate SSRT to a dopaminergic neurochemical marker in humans. The results support previous studies in humans showing a relationship between dopamine function and SSRT using pharmacological manipulations (Tannock et al., 1989; de Wit et al., 2002), indirect indicators of dopamine function measured by spontaneous eye-blink rate (Colzato et al., 2009), and observations of longer SSRTs in stimulant abusers (Monterosso et al., 2005; Colzato et al., 2007), who, as a group, exhibit low striatal D_2-like receptor availability. They also extend our observation of a negative correlation between self-reported impulsivity and striatal D_2/D_3 receptor availability in humans, particularly those who abuse methamphetamine (Lee et al., 2009), by showing a positive relationship between response inhibition and striatal D_2/D_3 receptor availability in healthy participants. Furthermore, this study is consistent with studies in which baseline striatal D_2-like receptor availability predicted impulsive behavior and rates of cocaine administration in drug-naive rodents (Dalley et al., 2007) and nonhuman primates (Nader et al., 2006).

The anatomical specificity (dorsal/ventral striatum) of the SSRT receptor availability correlations corroborate findings from rodent lesion and pharmacological studies suggesting that the nucleus accumbens does not participate in response inhibition (as measured by SSRT) (Eagle and Robbins, 2003a; Eagle et al., 2011), a distinction that coheres with a functional dissociation between the ability to "stop" an initiated response and "wait" for an impending reward as separate phenotypes of impulsivity served by dorsal and ventral striatum, respectively (Robinson et al., 2009). Further support for this distinction comes from observations of lower D_2/D_3 receptor availability in the ventral but not dorsal striatum of highly impulsive rats that exhibit greater premature responding (deficient "waiting") (Dalley et al., 2007) and studies showing that nucleus accumbens lesions induce more impulsive selections for sooner/smaller versus larger/later rewards (Cardinal et al., 2001). Nonetheless, though SSRT and receptor availability in the nucleus accumbens were not correlated in this study, measurement error might have contributed because the region is a small structure susceptible to partial volume effects in PET.

Our results are partially consistent with a model of striatal control of behavior that makes functional distinctions between dopamine receptor subtypes (Frank, 2005). This distinction posits that striatonigral neurons expressing primarily D_1 receptors facilitate "Go" responding whereas striatopallidal neurons expressing D_2 receptors support No-Go responses (Frank and O'Reilly, 2006; Frank et al., 2007). Although we did not measure D_1 receptor availability, the fact that D_2/D_3 receptor availability was related to SSRT and not Go RT generally supports this model.

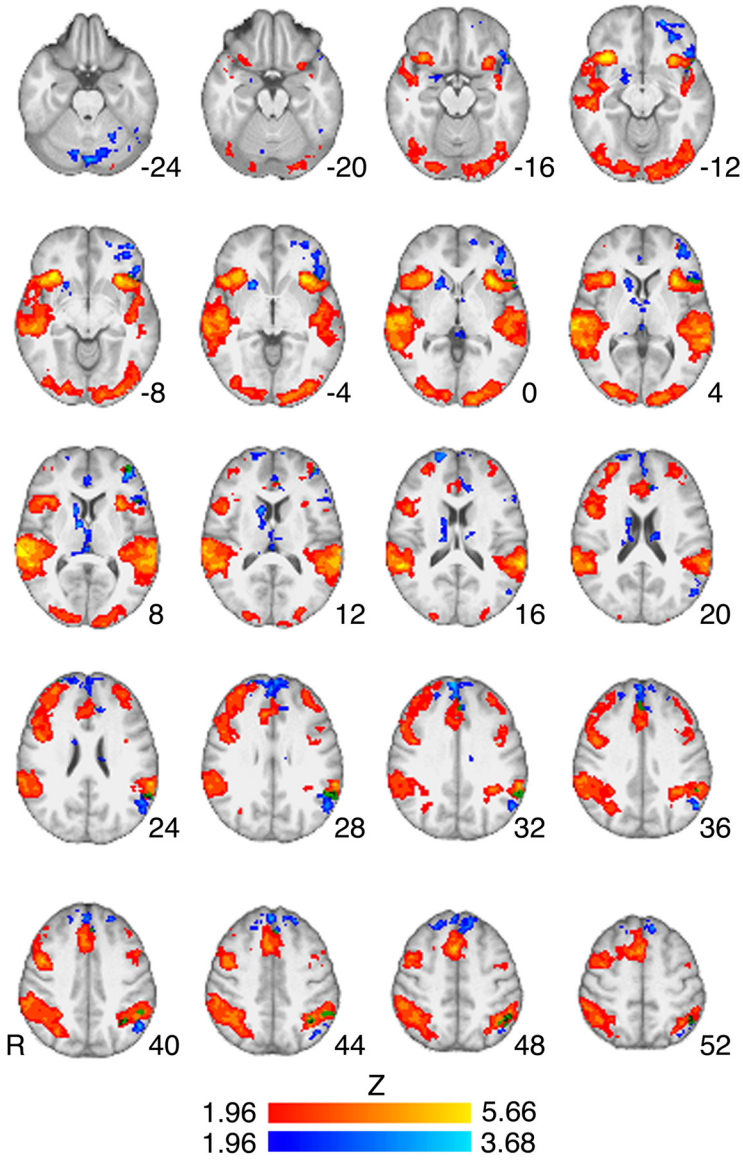

Figure 2. Successful Stop versus Go fMRI contrast and negative correlation with SSRT. *Z*-statistic map for Stop versus Go is represented by hot colors, and negative correlation of Stop versus Go and SSRT is represented by cool colors. Stop versus Go activations were found in regions typically reported in fMRI studies of the task, including right inferior frontal gyrus, pre-SMA, anterior cingulate, and the insula (Table 3 for list of regions). Clusters corresponding to the negative correlation between Stop versus Go and SSRT were found in the right caudate, putamen, superior frontal gyrus, and left orbitofrontal cortex (see Table 3 for full list of regions). No regions showed significant clusters for positive correlation with SSRT. *Z*-statistic maps were whole-brain, cluster-corrected (voxel height threshold, $Z > 1.96$; cluster-forming threshold, $p < 0.05$). *Z*-statistic maps are overlaid on the group mean high-resolution anatomical image. Numbers to the side of images represent *Z*-coordinates in MNI standard space. Images are presented in radiological orientation (right = left).

However, caution should be taken when considering these results with respect to the model. Assessments comparing studies of stop-signal and Go/No-Go tasks indicate clear dissociations in the pharmacology and neural circuitry underlying "action cancelation" (i.e., stopping) and "action restraint" (i.e., No-Go) (Eagle et al., 2008; Swick et al., 2011), suggesting that the two represent different processes. Thus, models drawing from Go/No-Go results may not generalize to SST findings. Moreover, pharmacological studies do not support a clear double-dissociation between receptor subtype and the two basic components of these tasks (i.e., Go and Stop/No-Go). Eagle et al. (2011) found that a D_2 receptor antagonist infused in the dorsal striatum slowed SSRTs but also slowed Go RTs, whereas a D_1 antagonist decreased SSRTs with no effect on Go RT. These results are mostly parallel with our findings but only partially consistent with the model, suggesting that, beyond separating receptor function by action inhibition and Go processes, models of striatal behavioral control may benefit from taking into account a balance of both D_1 and D_2 receptor activity in support of inhibitory control.

Further evidence for the role of D_2 receptors in stopping comes from a human genetic study linking a polymorphism that controls D_2 receptor expression (Zhang et al., 2007) and SSRT (Hamidovic et al., 2009). Although we could not directly distinguish between D_2 and D_3 receptor availability using [^{18}F]fallypride, our results in the dorsal striatum likely reflect involvement of D_2 receptors because dopamine receptors in this region in humans are primarily D_2, whereas the ventral striatum exhibits substantial D_3 receptor binding (Seeman et al., 2006; Searle et al., 2010).

Striatal D_2/D_3 receptor availability and response inhibition-related fMRI activation

Dorsal striatal D_2/D_3 receptor availability was related to fMRI activation associated with stopping. Previous fMRI and patient studies have identified key brain regions important for mediating SSRT. These include ventrolateral [right inferior frontal gyrus (rIFG)/anterior insula] and medial prefrontal [pre-SMA/anterior cingulate (ACC) cortex], subthalamic nucleus (Aron et al., 2003, 2007a; Chambers et al., 2009), and the striatum (Vink et al., 2005; Li et al., 2008; Jahfari et al., 2009; Boehler et al., 2010; Zandbelt and Vink, 2010). Within the striatum, the caudate nucleus shows greater activation during stopping with fast versus slow SSRTs (Li et al., 2008) and when participants are more likely to anticipate stopping (Vink et al., 2005; Jahfari et al., 2009; Zandbelt and Vink, 2010), highlighting its role in controlled execution of motor behavior (whether by preparing to stop, representing stopping rules, or implementing stopping itself). The relationship of this activation to dopaminergic function had not been previously established. The positive correlation between caudate D_2/D_3 receptor availability and Successful Stop versus Go activation reported here provides potential evidence for D_2-like neurotransmission underlying stopping-related caudate activation. However, since these correlations do not demonstrate a causal relationship, caudate D_2/D_3 receptor availability may be only an index of stopping ability and may not necessarily directly influence activation. Further studies are required for a definitive answer.

We also observed a positive relationship between activation in several prefrontal regions and caudate D_2/D_3 receptor availabil-

Table 3. Clusters from Successful Stop versus Go fMRI contrast and negative correlation with SSRT

Brain region	Hemisphere	Voxels	Maximum *Z*-statistic	*x*	*y*	*z*
Successful stop versus Go fMRI						
Anterior insula	R	1536	5.66	36	20	−10
Inferior frontal gyrus, pars opercularis			4.05	48	10	16
Precentral gyrus			4.32	46	4	42
Anterior insula[a]	L	699	5.24	−32	18	−6
Supplementary motor area/pre-supplementary motor area/rostral anterior cingulate[a]	R	585	4.71	4	14	48
Middle frontal gyrus/frontal pole	R	188	4.09	32	50	22
	L	221	3.53	−34	46	22
Superior temporal gyrus/supramarginal gyrus	R	3084	5.49	64	−34	8
	L	2364	5.32	−62	−42	16
Occipital pole	L	792	4.20	−16	−100	0
	R	188	4.09	32	50	22
Negative correlation of SSRT and Successful Stop versus Go fMRI						
Superior frontal gyrus[a]	R	1433	3.27	4	58	32
Frontal pole			2.92	18	62	16
Rostral anterior cingulate[a]			2.20	2	40	6
Inferior frontal gyrus, pars orbitalis[a]	L	1061	3.33	−40	46	6
Anterior orbital gyrus			3.28	−20	54	−12
Putamen	R	809	3.42	20	14	−2
Caudate			3.15	12	10	10
Thalamus			3.06	10	−4	8
Angular/supramarginal gyri	L	649	3.14	−50	−60	40
Lateral occipital gyrus			2.93	−50	−72	18
Cerebellum	R/L	2257	3.68	8	−84	−30

Z-statistics and *x*, *y*, and *z* MNI coordinates (mm) are from the location of peak voxel within each cluster (or local maxima within clusters, indicated by indented regions). *Z*-statistic maps were whole-brain cluster-corrected at $Z > 1.96$, $p < 0.05$. No regions showed significant clusters for positive correlation with SSRT.

[a]Regions showing overlap with whole-brain correlation of caudate BP_{ND} and Successful Stop versus Go fMRI (Figure 3, Table 4).

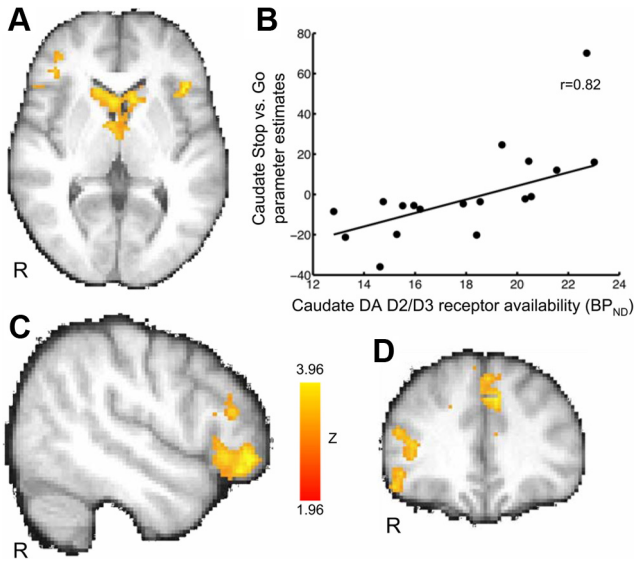

Figure 3. Correlations between caudate D_2/D_3 receptor availability (BP_{ND}) and fMRI contrast of Successful Stop versus Go ($n = 18$). Participants with greater caudate receptor D_2/D_3 receptor availability had greater activation in frontostriatal brain regions. Image shows *Z*-statistic map thresholded at $Z > 1.96$ (whole-brain, cluster-corrected threshold of $p < 0.05$) overlaid on the mean, spatially normalized anatomical image. ***A***, ***C***, ***D***, Bilateral caudate (***A***), right inferior frontal cortex/lateral occipital cortex (***C***, ***D***), and rostral anterior cingulate/superior frontal (medial portion) (***D***) regions of activation (see Table 4 for full list of regions). Images are presented in radiological orientation (right = left). MNI coordinates: transverse slice, $Z = 4$ (***A***); sagittal slice, $X = 50$ (***C***); and coronal slice, $Y = 34$ (***D***). R, Right. Color bar indicates *Z*-statistic range. ***B***, Scatterplot shows relationship between dopamine D_2/D_3 receptor availability and Successful Stop versus Go parameter estimates in anatomically defined caudate VOI ($r = 0.82$, $p = 0.00002$; without outlier: $r = 0.70$, $p = 0.002$). A weighted average of left and right caudate parameter estimates was used because the two were highly correlated ($r = 0.82$, $p < 0.0001$).

Table 4. Clusters from whole-brain positive correlation of caudate D_2/D_3 receptor availability (BP_{ND}) with Successful Stop versus Go fMRI contrast

Brain region	Hemisphere	Voxels	Maximum *Z*-statistic	*x*	*y*	*z*
Caudate	L/R	1173	3.49	12	16	8
Thalamus	R		2.98	6	−2	6
Superior frontal gyrus	R	496	3.12	22	48	32
Frontal pole/lateral orbitofrontal cortex	R	823	3.40	50	42	−8
Rostral anterior cingulate/superior frontal cortex (medial portion)	L/R	1099	3.78	0	48	38
Inferior frontal gyrus, pars opercularis/anterior insula	L	497	3.56	−42	16	−2
Middle frontal gyrus	L	504	3.47	−42	20	44
Cerebellum	L/R	1984	3.76	−6	−84	−32

L, Left; R, right. *Z*-statistics and *x*, *y*, and *z* MNI coordinates (mm) are from the location of peak voxel within each cluster (or local maxima within clusters, indicated by indented regions). *Z*-statistic maps were whole-brain cluster-corrected at $Z > 1.96$, $p < 0.05$. No regions showed significant clusters for negative correlation with BP_{ND}.

ity. These included the right superior frontal cortex, right lateral orbital/frontopolar cortex, left anterior insula, ACC, and paracingulate cortices. Insula and ACC activations are commonly reported in fMRI studies of response inhibition (Swick et al., 2011, for a meta-analysis) and have been identified in a "mega"-analysis of several Stop-signal fMRI datasets to negatively correlate with SSRT (Congdon et al., 2010). Activation in these regions overlapped across the Stop versus Go contrast and its correlation with BP_{ND} and SSRT, adding support for their role in response inhibition with potential mediation by dopamine receptor function.

We observed a correlation between striatal receptor availability and activation within two other prefrontal regions important for stopping, pre-SMA and rIFG, but with uncorrected, voxelwise thresholds (pre-SMA: $p < 0.005$; *x*, *y*, *z* = 6, 10, 62) (rIFG, pars opercularis: $p < 0.001$; *x*, *y*, *z* = 54, 24, 0),

providing only preliminary evidence for a relationship to dopamine receptor availability.

The correlation between ACC activation and caudate D_2/D_3 receptor availability further supports a dopaminergic influence on response inhibition given the direct connections between dorsal striatum and ACC (Haber and Knutson, 2010). It is possible that dopaminergic function influences the strength of frontostriatal functional connectivity (e.g., ACC–caudate strength) mediating SSRT (Jahfari et al., 2011), but this remains to be established.

Together with a PET study showing a positive relationship between striatal fMRI activation and dopamine release (Schott et al., 2008), this study provides evidence for an influence of striatal dopamine neurotransmission on blood oxygen level-dependent (BOLD) responses. However, the coupling of dopamine receptor availability and the neurovasculature on which the BOLD signal depends is not fully understood. Rodent studies indicate that indirect dopamine agonists (e.g., amphetamine) increase regional cerebral blood volume (rCBV), a strong correlate of BOLD fMRI, by a primarily nonvascular action; however, direct D_2/D_3 agonists reduce rCBV and antagonize rCBV enhancement induced by indirect agonists (Chen et al., 2005; Choi et al., 2006). These observations suggest that striatal D_2/D_3 receptor availability would be negatively related to fMRI responses associated with dopamine release. The discrepancy between the positive relationship observed in humans and these findings using systemic dopaminergic manipulations may reflect a lack of correspondence between the animal and human models or differences between actions of activity-related dopamine release in a discreet network compared with globally induced pharmacological effects.

Conclusions

In summary, we show that dopamine receptor availability is related to response inhibition and activation of related frontostriatal circuitry in humans. Although SSRT is primarily considered a measure of motor-response inhibition, some evidence suggests that it is related to other forms of self-control, such as drug craving in stimulant abusers and regulation of emotional states (Cohen and Lieberman, 2010; Tabibnia et al., 2011) and is predictive of substance abuse vulnerability (Nigg et al., 2006; Ersche et al., 2012). Several psychiatric populations (e.g., persons with attention deficit hyperactivity disorder, schizophrenia, drug dependence) show irregular dopamine function combined with impulsive behavior as common phenotypes. This study provides evidence for a direct link between the two, affording a basis for pharmacotherapeutic treatments that target specific dopamine receptor function for disorders marked by poor response inhibition.

References

Andersson JLR, Jenkinson M, Smith S (2007a) Non-linear optimisation. Oxford, UK: FMRIB Centre TR07JA1 (www.fmrib.ox.ac.uk/analysis/techrep).

Andersson J, Jenkinson M, Smith S (2007b) Non-linear registration, aka spatial normalization. Oxford, UK: FMRIB Centre TR07JA2 (www.fmrib.ox.ac.uk/analysis/techrep).

Ardekani BA, Braun M, Hutton BF, Kanno I, Iida H (1995) A fully automatic multimodality image registration algorithm. J Comput Assist Tomogr 19:615–623.

Aron AR, Poldrack RA (2006) Cortical and subcortical contributions to stop signal response inhibition: role of the subthalamic nucleus. J Neurosci 26:2424–2433.

Aron AR, Fletcher PC, Bullmore ET, Sahakian BJ, Robbins TW (2003) Stop-signal inhibition disrupted by damage to right inferior frontal gyrus in humans. Nat Neurosci 6:115–116.

Aron AR, Behrens TE, Smith S, Frank MJ, Poldrack RA (2007a) Triangulating a cognitive control network using diffusion-weighted magnetic resonance imaging (MRI) and functional MRI. J Neurosci 27:3743–3752.

Aron AR, Durston S, Eagle DM, Logan GD, Stinear CM, Stuphorn V (2007b) Converging evidence for a fronto-basal-ganglia network for inhibitory control of action and cognition. J Neurosci 27:11860–11864.

Band GP, van der Molen MW, Logan GD (2003) Horse-race model simulations of the stop-signal procedure. Acta Psychol (Amst) 112:105–142.

Beckmann CF, Jenkinson M, Smith SM (2003) General multilevel linear modeling for group analysis in FMRI. Neuroimage 20:1052–1063.

Boehler CN, Appelbaum LG, Krebs RM, Hopf JM, Woldorff MG (2010) Pinning down response inhibition in the brain–conjunction analyses of the stop-signal task. Neuroimage 52:1621–1632.

Buckholtz JW, Treadway MT, Cowan RL, Woodward ND, Li R, Ansari MS, Baldwin RM, Schwartzman AN, Shelby ES, Smith CE, Kessler RM, Zald DH (2010) Dopaminergic network differences in human impulsivity. Science 329:532.

Cardinal RN, Pennicott DR, Sugathapala CL, Robbins TW, Everitt BJ (2001) Impulsive choice induced in rats by lesions of the nucleus accumbens core. Science 292:2499–2501.

Chambers CD, Garavan H, Bellgrove MA (2009) Insights into the neural basis of response inhibition from cognitive and clinical neuroscience. Neurosci Biobehav Rev 33:631–646.

Cohen JR, Lieberman MD (2010) The common neural basis of exerting self-control in multiple domains. In: Self-control (Trope Y HR, Ochsner K, ed), pp 141–160. New York: Oxford UP.

Colzato LS, van den Wildenberg WP, Hommel B (2007) Impaired inhibitory control in recreational cocaine users. PLoS One 2:e1143.

Colzato LS, van den Wildenberg WP, van Wouwe NC, Pannebakker MM, Hommel B (2009) Dopamine and inhibitory action control: evidence from spontaneous eye blink rates. Exp Brain Res 196:467–474.

Congdon E, Lesch KP, Canli T (2008) Analysis of DRD4 and DAT polymorphisms and behavioral inhibition in healthy adults: implications for impulsivity. Am J Med Genet B Neuropsychiatr Genet 147B:27–32.

Congdon E, Mumford JA, Cohen JR, Galvan A, Aron AR, Xue G, Miller E, Poldrack RA (2010) Engagement of large-scale networks is related to individual differences in inhibitory control. Neuroimage 53:653–663.

Dalley JW, Fryer TD, Brichard L, Robinson ES, Theobald DE, Lääne K, Peña Y, Murphy ER, Shah Y, Probst K, Abakumova I, Aigbirhio FI, Richards HK, Hong Y, Baron JC, Everitt BJ, Robbins TW (2007) Nucleus accumbens D2/3 receptors predict trait impulsivity and cocaine reinforcement. Science 315:1267–1270.

de Wit H, Enggasser JL, Richards JB (2002) Acute administration of D-amphetamine decreases impulsivity in healthy volunteers. Neuropsychopharmacology 27:813–825.

Duvernoy HM (1999) The human brain: surface, three-dimensional sectional anatomy with MRI, and blood supply, Ed 2. Vienna: Springer.

Eagle DM, Robbins TW (2003a) Lesions of the medial prefrontal cortex or nucleus accumbens core do not impair inhibitory control in rats performing a stop-signal reaction time task. Behav Brain Res 146:131–144.

Eagle DM, Robbins TW (2003b) Inhibitory control in rats performing a stop-signal reaction-time task: effects of lesions of the medial striatum and D-amphetamine. Behav Neurosci 117:1302–1317.

Eagle DM, Bari A, Robbins TW (2008) The neuropsychopharmacology of action inhibition: cross-species translation of the stop-signal and go/no-go tasks. Psychopharmacology (Berl) 199:439–456.

Eagle DM, Wong JC, Allan ME, Mar AC, Theobald DE, Robbins TW (2011) Contrasting roles for dopamine D1 and D2 receptor subtypes in the dorsomedial striatum but not the nucleus accumbens core during behavioral inhibition in the stop-signal task in rats. J Neurosci 31:7349–7356.

Ersche KD, Jones PS, Williams GB, Turton AJ, Robbins TW, Bullmore ET (2012) Abnormal brain structure implicated in stimulant drug addiction. Science 335:601–604.

First MB, Spitzer RL, Gibbon M, Williams JBW (2002) Structured clinical interview for DSM-IV Axis I disorders, research version, patient edition (SCID-I/P, v2.0). New York: Biometrics Research Department, New York State Psychiatric Institute.

Frank MJ (2005) Dynamic dopamine modulation in the basal ganglia: a neurocomputational account of cognitive deficits in medicated and nonmedicated Parkinsonism. J Cogn Neurosci 17:51–72.

Frank MJ, O'Reilly RC (2006) A mechanistic account of striatal dopamine function in human cognition: psychopharmacological studies with cabergoline and haloperidol. Behav Neurosci 120:497–517.

Frank MJ, Santamaria A, O'Reilly RC, Willcutt E (2007) Testing computational

models of dopamine and noradrenaline dysfunction in attention deficit/hyperactivity disorder. Neuropsychopharmacology 32:1583–1599.
Haber SN, Knutson B (2010) The reward circuit: linking primate anatomy and human imaging. Neuropsychopharmacology 35:4–26.
Hamidovic A, Dlugos A, Skol A, Palmer AA, de Wit H (2009) Evaluation of genetic variability in the dopamine receptor D2 in relation to behavioral inhibition and impulsivity/sensation seeking: an exploratory study with d-amphetamine in healthy participants. Exp Clin Psychopharmacol 17:374–383.
Jahfari S, Stinear CM, Claffey M, Verbruggen F, Aron AR (2010) Responding with restraint: what are the neurocognitive mechanisms? J Cogn Neurosci 22:1479–1492.
Jahfari S, Waldorp L, van den Wildenberg WP, Scholte HS, Ridderinkhof KR, Forstmann BU (2011) Effective connectivity reveals important roles for both the hyperdirect (fronto-subthalamic) and the indirect (fronto-striatal-pallidal) frontobasal ganglia pathways during response inhibition. J Neurosci 31:6891–6899.
Jenkinson M, Smith S (2001) A global optimisation method for robust affine registration of brain images. Med Image Anal 5:143–156.
Jenkinson M, Bannister P, Brady M, Smith S (2002) Improved optimization for the robust and accurate linear registration and motion correction of brain images. Neuroimage 17:825–841.
Koob GF, Volkow ND (2010) Neurocircuitry of addiction. Neuropsychopharmacology 35:217–238.
Lammertsma AA, Hume SP (1996) Simplified reference tissue model for PET receptor studies. Neuroimage 4:153–158.
Lee B, London ED, Poldrack RA, Farahi J, Nacca A, Monterosso JR, Mumford JA, Bokarius AV, Dahlbom M, Mukherjee J, Bilder RM, Brody AL, Mandelkern MA (2009) Striatal dopamine D_2/D_3 receptor availability is reduced in methamphetamine dependence and is linked to impulsivity. J Neurosci 29:14734–14740.
Li CS, Yan P, Sinha R, Lee TW (2008) Subcortical processes of motor response inhibition during a stop signal task. Neuroimage 41:1352–1363.
Liu TT, Frank LR, Wong EC, Buxton RB (2001) Detection power, estimation efficiency, and predictability in event-related fMRI. Neuroimage 13:759–773.
Logan GD, Cowan WB (1984) On the ability to inhibit thought and action—a theory of an act of control. Psychol Rev 91:295–327.
Logan GD, Schachar RJ, Tannock R (1997) Impulsivity and inhibitory control. Psychol Sci 8:60–64.
Mirabella G, Iaconelli S, Romanelli P, Modugno N, Lena F, Manfredi M, Cantore G (2012) Deep brain stimulation of subthalamic nuclei affects arm response inhibition in Parkinson's patients. Cereb Cortex 22:1124–1132.
Monterosso JR, Aron AR, Cordova X, Xu J, London ED (2005) Deficits in response inhibition associated with chronic methamphetamine abuse. Drug Alcohol Depend 79:273–277.
Mukherjee J, Yang ZY, Das MK, Brown T (1995) Fluorinated benzamide neuroleptics, III: development of (S)-N-[(1-allyl-2-pyrrolidinyl)methyl]-5-(3-[18F]fluoropropyl)-2, 3-dimethoxybenzamide as an improved dopamine D-2 receptor tracer. Nucl Med Biol 22:283–296.
Nader MA, Morgan D, Gage HD, Nader SH, Calhoun TL, Buchheimer N, Ehrenkaufer R, Mach RH (2006) PET imaging of dopamine D2 receptors during chronic cocaine self-administration in monkeys. Nat Neurosci 9:1050–1056.
Nichols TE, Holmes AP (2002) Nonparametric permutation tests for functional neuroimaging: a primer with examples. Hum Brain Mapp 15:1–25.
Nichols T, Brett M, Andersson J, Wager T, Poline JB (2005) Valid conjunction inference with the minimum statistic. Neuroimage 25:653–660.
Nigg JT, Wong MM, Martel MM, Jester JM, Puttler LI, Glass JM, Adams KM, Fitzgerald HE, Zucker RA (2006) Poor response inhibition as a predictor of problem drinking and illicit drug use in adolescents at risk for alcoholism and other substance use disorders. J Am Acad Child Adolesc Psychiatry 45:468–475.
R Development Core Team (2011) R: A language and environment for statistical computing. Vienna, Austria: R Foundation for Statistical Computing (http://www.R-project.org).
Rieger M, Gauggel S, Burmeister K (2003) Inhibition of ongoing responses following frontal, nonfrontal, and basal ganglia lesions. Neuropsychology 17:272–282.
Robinson ES, Eagle DM, Economidou D, Theobald DE, Mar AC, Murphy ER, Robbins TW, Dalley JW (2009) Behavioural characterisation of high impulsivity on the 5-choice serial reaction time task: specific deficits in "waiting" versus "stopping". Behav Brain Res 196:310–316.
Schott BH, Minuzzi L, Krebs RM, Elmenhorst D, Lang M, Winz OH, Seidenbecher CI, Coenen HH, Heinze HJ, Zilles K, Düzel E, Bauer A (2008) Mesolimbic functional magnetic resonance imaging activations during reward anticipation correlate with reward-related ventral striatal dopamine release. J Neurosci 28:14311–14319.
Searle G, Beaver JD, Comley RA, Bani M, Tziortzi A, Slifstein M, Mugnaini M, Griffante C, Wilson AA, Merlo-Pich E, Houle S, Gunn R, Rabiner EA, Laruelle M (2010) Imaging dopamine D3 receptors in the human brain with positron emission tomography, [11C]PHNO, and a selective D3 receptor antagonist. Biol Psychiatry 68:392–399.
Seeman P, Wilson A, Gmeiner P, Kapur S (2006) Dopamine D2 and D3 receptors in human putamen, caudate nucleus, and globus pallidus. Synapse 60:205–211.
Smith SM, Nichols TE (2009) Threshold-free cluster enhancement: addressing problems of smoothing, threshold dependence and localisation in cluster inference. Neuroimage 44:83–98.
Swann N, Poizner H, Houser M, Gould S, Greenhouse I, Cai W, Strunk J, George J, Aron AR (2011) Deep brain stimulation of the subthalamic nucleus alters the cortical profile of response inhibition in the beta frequency band: a scalp EEG study in Parkinson's disease. J Neurosci 31:5721–5729.
Swanson JM, Kinsbourne M, Nigg J, Lanphear B, Stefanatos GA, Volkow N, Taylor E, Casey BJ, Castellanos FX, Wadhwa PD (2007) Etiologic subtypes of attention-deficit/hyperactivity disorder: brain imaging, molecular genetic and environmental factors and the dopamine hypothesis. Neuropsychol Rev 17:39–59.
Swick D, Ashley V, Turken U (2011) Are the neural correlates of stopping and not going identical? Quantitative meta-analysis of two response inhibition tasks. Neuroimage 56:1655–1665.
Tabibnia G, Monterosso JR, Baicy K, Aron AR, Poldrack RA, Chakrapani S, Lee B, London ED (2011) Different forms of self-control share a neurocognitive substrate. J Neurosci 31:4805–4810.
Tannock R, Schachar RJ, Carr RP, Chajczyk D, Logan GD (1989) Effects of methylphenidate on inhibitory control in hyperactive children. J Abnorm Child Psychol 17:473–491.
Tohka J, Foerde K, Aron AR, Tom SM, Toga AW, Poldrack RA (2008) Automatic independent component labeling for artifact removal in fMRI. Neuroimage 39:1227–1245.
Vandehey NT, Moirano JM, Converse AK, Holden JE, Mukherjee J, Murali D, Nickles RJ, Davidson RJ, Schneider ML, Christian BT (2010) High-affinity dopamine D2/D3 PET radioligands 18F-fallypride and 11C-FLB457: a comparison of kinetics in extrastriatal regions using a multiple-injection protocol. J Cereb Blood Flow Metab 30:994–1007.
Verbruggen F, Logan GD (2008) Response inhibition in the stop-signal paradigm. Trends Cogn Sci 12:418–424.
Vink M, Kahn RS, Raemaekers M, van den Heuvel M, Boersma M, Ramsey NF (2005) Function of striatum beyond inhibition and execution of motor responses. Hum Brain Mapp 25:336–344.
Volkow ND, Chang L, Wang GJ, Fowler JS, Ding YS, Sedler M, Logan J, Franceschi D, Gatley J, Hitzemann R, Gifford A, Wong C, Pappas N (2001) Low level of brain dopamine D2 receptors in methamphetamine abusers: association with metabolism in the orbitofrontal cortex. Am J Psychiatry 158:2015–2021.
Woolrich M (2008) Robust group analysis using outlier inference. Neuroimage 41:286–301.
Woolrich MW, Ripley BD, Brady M, Smith SM (2001) Temporal autocorrelation in univariate linear modeling of FMRI data. Neuroimage 14:1370–1386.
Woolrich MW, Behrens TE, Beckmann CF, Jenkinson M, Smith SM (2004) Multilevel linear modelling for FMRI group analysis using Bayesian inference. Neuroimage 21:1732–1747.
Worsley KJ, Evans AC, Marrett S, Neelin P (1992) A three-dimensional statistical analysis for CBF activation studies in human brain. J Cereb Blood Flow Metab 12:900–918.
Wu Y, Carson RE (2002) Noise reduction in the simplified reference tissue model for neuroreceptor functional imaging. J Cereb Blood Flow Metab 22:1440–1452.
Zandbelt BB, Vink M (2010) On the role of the striatum in response inhibition. PLoS One 5:e13848.
Zhang Y, Bertolino A, Fazio L, Blasi G, Rampino A, Romano R, Lee ML, Xiao T, Papp A, Wang D, Sadée W (2007) Polymorphisms in human dopamine D2 receptor gene affect gene expression, splicing, and neuronal activity during working memory. Proc Natl Acad Sci U S A 104:20552–20557.